Nano Research

Open Access

Research Article

Observation of memristive behavior in PDMS-glass nanofluidic chip

Weiling Sun[1], Yike Xiao[1], Pingyuan Yan[1], Fei Sun[2], Xuan Zhang[2], Chuanxiang Sheng[3], Qi Wang[1] ✉, and Yefeng Yu[1] ✉

[1] School of Microelectronics, Nanjing University of Science and Technology, Nanjing 210094, China
[2] Key Laboratory of New Membrane Materials, Ministry of Industry and Information Technology, School of Environmental and Biological Engineering, Nanjing University of Science and Technology, Nanjing 210094, China
[3] Department of Optical Science and Engineering, School of Information Science and Technology, Fudan University, Shanghai 200433, China

Cite this article: *Nano Research*, **2025**, *18*, 94907098. https://doi.org/10.26599/NR.2025.94907098

ABSTRACT: Nanofluidic memristors, which use ions in electrolyte solutions as carriers, have been developed rapidly and brought new opportunities for the development of neuromorphic devices. Utilizing the transport and accumulation of ions in nanochannels to process information is an endeavor to realize the nanofluidic memristor. In this study, we report a new nanofluidic memristor, which is a polydimethylsiloxane (PDMS)-glass chip with two platinum (Pt) electrodes and well-aligned multi-nanochannels within PDMS for ion enrichment and depletion. The device not only exhibits typical bipolar memristive behavior and ion current rectification (ICR) but also demonstrates excellent endurance, maintaining stable performance after 100 sweep cycles. We systematically investigate the key factors affecting ion transport behavior in this memristor. The results show that the ICR ratio of the current–voltage (*I*–*V*) hysteresis curves decreases with increasing scan rate and solution concentration. Zeta potential measurements are introduced to reveal that the PDMS surface carries more negative charges in higher pH solutions, resulting in more pronounced memristive and ICR effects. Furthermore, our memristor can simulate short-term synaptic plasticity, such as paired-pulse facilitation (PPF) and paired-pulse depression (PPD), with a relatively low energy consumption of 12 pJ per spike per channel. Potentially, the inherent accessibility and robustness of our nanofluidic memristors facilitate the optimization of device structure and performance. These important observations and investigations lay a foundation for advancing energy-saving and efficient neuromorphic computing.

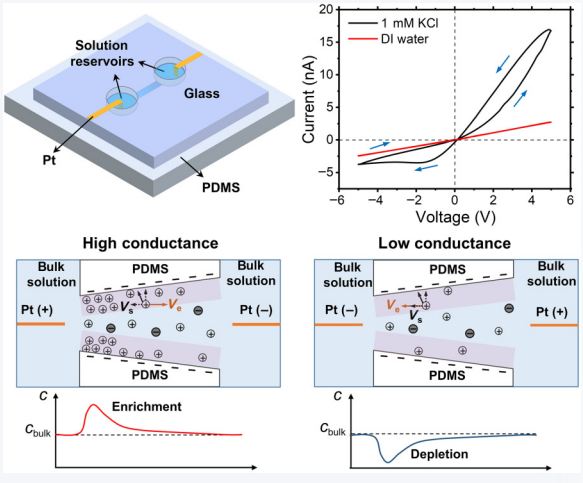

KEYWORDS: polydimethylsiloxane (PDMS)-glass chip, nanofluidic memristor, nanochannel, short-term synaptic plasticity (STP)

1 Introduction

A memristor, short for "memory resistor", is an electronic device whose conductivity is dependent on the amount of charge that passes through it [1, 2]. The resistance of memristors can be programmed to represent different synaptic weights, which enables them to process and store information similarly to biological neurons. Leveraging this capability for in-memory computing and parallel processing of complex information, memristors are emerging as a promising candidate for neuromorphic computing [3]. Since the first solid-state memristor being demonstrated by Hewlett–Packard laboratories in 2008 [4], various devices with memory effects based on phase transitions, redox reactions, ferroelectric polarization, or spin-polarized tunneling have emerged [5–7]. However, the energy consumption of the solid-state memristors is still not comparable to those of biological neurons with ions as carriers [8]. Thus, developing artificial fluidic memristors with ions as carriers becomes a new direction for researchers to explore and has recently drawn considerable attention. The initial evidence for the memory effect in fluidics emerged from impedance measurements of a glass nanopipette, which revealed hysteresis in the current–voltage (*I*–*V*) curves, thus

Received: August 31, 2024; **Revised:** October 22, 2024
Accepted: October 28, 2024

✉Address correspondence to Yefeng Yu, yf_yu@njust.edu.cn; Qi Wang, qi.wang@njust.edu.cn

substantiating the existence of memristive effect in this system [9, 10]. Subsequently, a variety of fluidic memristors based on diverse mechanisms have been proposed, such as interface movement [11], biomolecule insertion [12], concentration polarization [13], etc.

However, most of these emerging devices face with certain challenges such as high operating voltages or unreliability due to environmental sensitivity. More generally, a challenge is to replicate the mechanism found in biological systems, where the transport and accumulation of solvated ions in water are used for information processing and memory formation (Fig. 1(a)). Recently, Xiong et al. [14] and Robin et al. [15, 16] have experimentally demonstrated nanofluidic memristors based on potential-dependent ion enrichment and depletion through electrostatic interaction with the charged surface of a nanochannel. They can operate in a wide range of parameters—particularly salt concentration and pH and realize more complex neuromorphic functions at low power consumption. However, these nanofluidic memristors often involve complicated fabrication techniques, which may limit the reproducibility and independent verification of research. Therefore, it is essential to develop a nanofluidic memristor that is both readily accessible and demonstrates robust performance. In this study, we report a new nanofluidic memristor which is a polydimethylsiloxane (PDMS)-glass chip with two Pt electrodes and a nanochannel array for ion enrichment and depletion. The employment of well-aligned multi-nanochannels fabricated on PDMS aims to reduce the operating voltage and hence the energy consumption of the device. We use various potential scan rates and solution concentrations in the *I*–*V* electrical measurement to explore their effects on the ion transport behavior in this device. The results and the intrinsic mechanism are discussed in detail. Additionally, the zeta potential measurements and the pH adjustment experiments are performed to explore the influence of the surface charge density on the memristive and ion current rectification (ICR) effects. Finally, we try to modulate its conductance with voltage pulses to explore whether the device has the ability to mimic synaptic function. These investigations provide a significant addition to our understanding of nanofluidic memristors based on ion enrichment and depletion and contribute to the exploration of the practical application potential of these devices in neuromorphic computing.

2 Experiments

2.1 Device fabrication

The polystyrene (PS) Petri dish with diameter of 35 mm is filled with 3 mL ethanol and placed onto the hot plate with the temperature of 60 °C. The evaporated ethanol vapor interacts with the Petri dish lid and a nanochannel array is formed on the inner surface after 6 h. The Smooth-on 305 liquid plastic (1A:1B by volume) is well mixed and poured onto the inner surface of the PS lid. It is partially solidified after 40 min at room temperature. Subsequently, the plastic mold is removed from the PS lid and placed on a hot plate at 60 °C for 1-h solidification. Then, a mixture of PDMS precursor and curing agent (10:1 by weight) is poured onto the plastic mold. The mixture is then left at room temperature for 10 min (or degassed for 5 min) to eliminate gas bubbles. Finally, the PDMS is cured on a hot plate at 85 °C for 2 h. To enhance the bonding strength between the cured PDMS and the soda-lime glass surface, both surfaces are subjected to an ultraviolet (UV)/ozone (UVO) treatment for 30 min. Following this treatment, the PDMS is carefully aligned and irreversibly bonded to the glass. The size of the glass is 12 mm × 12 mm × 0.7 mm and two holes in the glass are created by laser cutting to act as solution reservoirs.

2.2 Electrical measurement

The electrical properties of the PDMS nanofluidic chip are measured at room temperature using the direct current (DC) sweep mode of a semiconductor device parameter analyzer (4200A, Keithley). The applied voltage is swept from 0 → 5 → 0 → −5 → 0 V. The synaptic function of the device is demonstrated by applying multiple positive triangular waves or negative triangular waves. The scanning electron microscopy (SEM) image of the PDMS nanochannel is obtained using a field emission SEM (JSM-7800F PRIME) at an accelerating voltage of 3 kV. The zeta potential is measured with an ATON PAAR SURPASS 3 electrokinetic analyzer at pH 7.

3 Results and discussion

3.1 PDMS-glass nanofluidic chip

The schematic of the nanofluidic chip is shown in Figs. 1(b) and

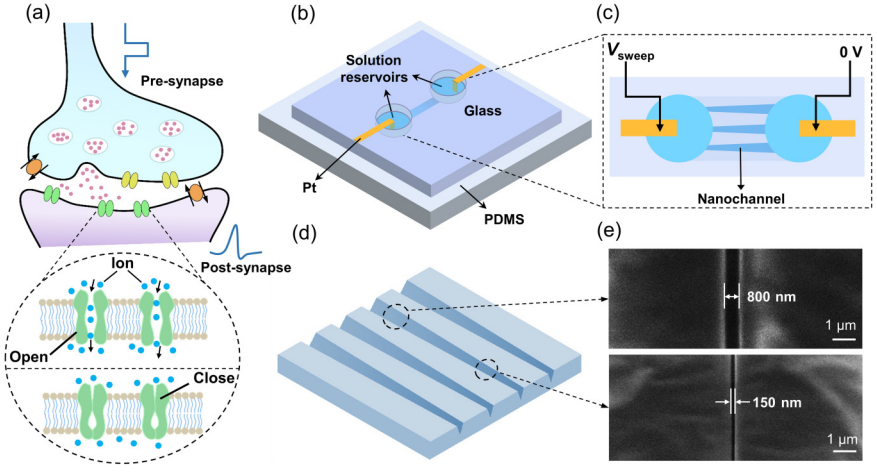

Figure 1 PDMS-glass nanofluidic chip. (a) Schematic of a biological synapse. (b) Schematic and (c) top view of the PDMS nanofluidic chip. (d) Schematic and (e) SEM images of the nanochannels fabricated by the crack-based lithography-free approach on the PDMS surface.

1(c), which consists of the PDMS layer with nanochannels, the soda-lime glass layer with two holes as solution reservoirs and a pair of Pt electrodes to apply voltages. The photograph and the SEM image of the device are shown in Figs. S1(a) and S1(b) in the Electronic Supplementary Material (ESM). As described in detail in the Section 2.1, a crack-based lithography-free approach is used to fabricated the nanochannels within PDMS (Fig. 1(d)) [17]. We have made a dent inside the PS lid near the edge, so that almost all the cracks are generated at this artificial defect and propagate to the other end of the PS lid. Most critically, surface swelling and the subsequent release of surface tension on the PS surface layers are considered to be the driving forces. As shown in Fig. 1(e), the morphology of a single PDMS nanochannel observed by SEM shows that it is asymmetrical with a non-uniform width. Specifically, the average channel widths at both ends are approximately 800 and 150 nm respectively. This is due to the higher stress concentration near the defect, which causes the crack size to decrease as the crack propagate farther away [18]. Figure S1(d) in the ESM presents the width distribution of the channel opening exposed to two reservoirs and the average widths are approximately 421 and 172 nm respectively. This asymmetry and width variation is the main reason for the memristive and ICR effects observed in the electrical measurements.

3.2 The hysteresis effect

Representative current responses of the nanofluidic chip under DC sweep mode (0 → 5 → 0 → −5 → 0 V) are shown in Fig. 2. Figure 2(a) shows the corresponding *I*–*V* curves for devices with 1 mM KCl solution and deionized (DI) water. The device with KCl solution (Fig. 2(a), black) exhibits typical bipolar memristive behavior, characterized by a self-crossing hysteresis loop. The conductance of the device changes gradually from low to high during the forward voltage sweep and then slowly returns to its initial value when the voltage polarity is reversed (Fig. 2(b)). Meanwhile, the *I*–*V* curve shows an obvious ICR behavior [19, 20], where the conductivity is higher at positive than at negative polarities of the same bias magnitude, resulting in an asymmetric current–voltage response. In comparison, the device with deionized water only yields a nearly linear ohmic *I*–*V* curve (Fig. 2(a), red). By magnifying the *I*–*V* curve of the DI water between 0.8–2.0 V (Fig. S2(f) in the ESM), a small hysteresis loop is observed, which may be caused by the water electrolysis with Pt electrodes. Comparing this hysteresis curve with that observed in 1 mM KCl solution (Fig. S2(e) in the ESM), the contribution of water electrolysis to the memristive hysteresis is only about 0.55%. Therefore, the effect of the water electrolysis on the memristive effect of the device can be neglected. The influence of channel size on the water electrolysis is also presented in Figs. S2(a)–S2(c) in the ESM. As the channel size reaches the micrometer scale or larger, water electrolysis becomes significant, leading to high currents (μA) and noticeable non-linearity in the *I*–*V* curves. While in nanochannels, electrolysis is minimal, generating a low current (nA) and an almost linear *I*–*V* response. These results demonstrate the essential role of salt ions in the memristive effect of our devices. Figure S4 in the ESM shows the *I*–*V* curves of the device with a series of different scan rates of the applied voltage. As the scan rate increases, the degree of nonlinearity of the curves decreases and the area of the hysteresis loop shrinks, which aligns with the memristive effects described in electronics [4, 21]. Additionally, it is observed that the hysteresis curve does not pass through the origin but is separated into two loops by a non-zero cross point at a positive bias. As the scan rate increases, the cross point shifts to a more positive value. Furthermore, the device exhibits good endurance in DC sweep mode, maintaining stable performance after 100 sweep cycles, as shown in Fig. 2(c). Figure

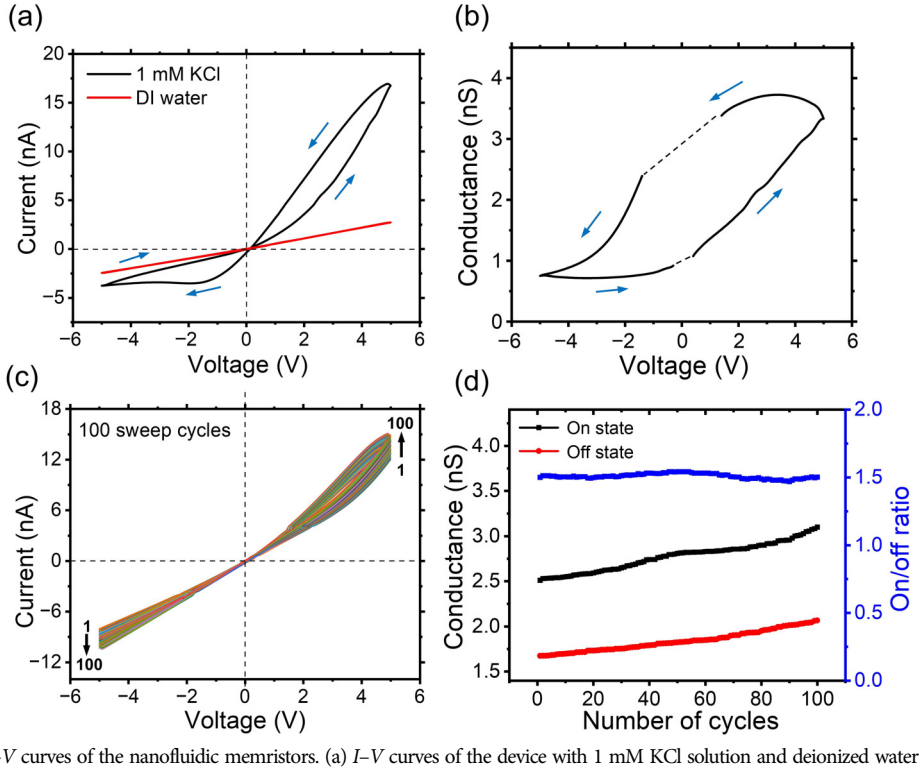

Figure 2 Experimental *I*–*V* curves of the nanofluidic memristors. (a) *I*–*V* curves of the device with 1 mM KCl solution and deionized water at a scan rate of 0.07 V/s. The blue arrows indicate the potential scan direction. (b) Conductance–voltage (*G*–*V*) curve of the nanofluidic memristor with 1 mM KCl solution from (a). (c) A total of 100 *I*–*V* sweep cycles of the device with 1 mM KCl solution. (d) Distribution of high/low conductance of the on/off states and on/off ratio from (c).

2(d) shows the distribution of high/low conductance values and on/off ratio extracted from the cycles. The values of the conductance drift (ΔG) versus the initial values (G_0), $\Delta G/G_0$, for the two states are approximately 20% and 29%, while the on/off ratio exhibits only a minor shift, maintaining around 1.5 throughout the 100 cycles. This result demonstrates the good stability of our device during the cyclic sweeps.

3.3 The memristive mechanism

With respect to the intrinsic mechanism underlying the observed memristive and ICR effects, we propose that the asymmetric geometry of the negatively charged PDMS nanochannels significantly influences the ion transport behavior in our device. Common materials used to fabricate nanochannels, such as glass and PDMS, typically develop a negatively charged surface upon contact with aqueous solutions [22]. This negative surface charge repels anions and attracts cations in the solution, forming an electrical double layer (EDL) [23], as shown in the purple region of Figs. 3(a) and 3(b). Due to the asymmetry of the nanochannel, the surface electric field has a component V_s in the mass transport direction, which superimposes with the external bias V_e, polarizing the ion concentration profile. In the specific case where V_e balances out V_s, the potential-induced net polarization is zero [24]. At a relatively positive bias potential, the negative surface charges and the external potential facilitate the cations to migrate into the nanochannel, resulting in ion enrichment in the EDL region, as shown in Fig. 3(a). Conversely, in Fig. 3(b), the external electric field leads to ion depletion in the EDL region of the nanochannel at a relatively negative bias [25]. Therefore, the cross point of I–V hysteresis curve represents the boundary of the potential-induced ion enrichment and depletion within the nanochannels. This ion enrichment and depletion will result in the high and low conductance states, respectively, known as ion current rectification. The hysteresis effect is due to the slower redistribution of ions compared to the variation of the applied potential that is being swept at the respective scan rates [26]. The ion redistribution corresponds to changes of ion concentration within the nanochannels. In comparison with the steady-state current responses under bias at a low scan rate, when the scan rate is faster, the ions inside the nanochannel do not have sufficient time to redistribute accordingly. Consequently, the conductance changes minimally and the area of the hysteresis loop shrinks.

As mentioned above, the electrokinetic ions transport in nanochannels is determined by the combined effects of externally applied electric fields and intrinsic surface electric fields. Ion enrichment or depletion in nanochannels is induced by electrostatic interactions with surface charges. Theoretically, the degree of ion enrichment increases with increasing surface charge density [27]. The memristive phenomenon diminish if the surface charges are neutralized, even in nanochannels with asymmetric geometries. Here, we investigate the effect of poly(sodium-p-styrenesulfonate) (PSS) on surface modification of PDMS. First, the PDMS is immersed in PSS solution (5 wt.%) for 6 h. As an anionic surfactant, PSS adsorbs onto the PDMS, resulting in a negatively charged and hydrophilic surface [28]. Then, the treated PDMS is subjected to zeta potential measurement to reveal the surface charge characteristics in solutions. To investigate the influence of UVO treatment before bonding on PSS modified PDMS, the zeta

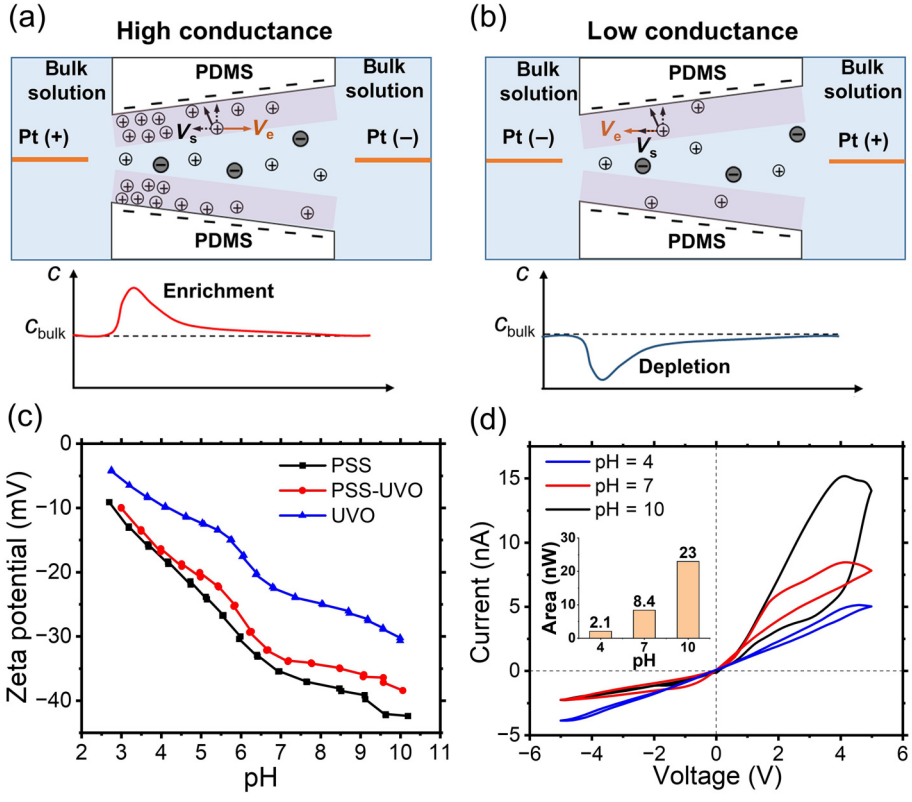

Figure 3 The operation mechanism and the effect of surface charge. (a) and (b) Potential-induced ion enrichment and depletion in an asymmetric charged nanochannel, resulting in high and low conductance. The dashed line indicates the bulk concentration of KCl solution. (c) Dependence of the zeta potential of the PSS-treated, PSS-UVO-treated and UVO-treated PDMS surfaces on the pH value of the solution. (d) I–V curves of the device fabricated with PSS-modified PDMS with 1 mM KCl solution at different pH values. The inset shows the hysteresis area of the I–V curves at three pH values.

potentials of the PSS-UVO-treated PDMS and UVO-treated PDMS have also been provided (Fig. 3(c)). The zeta potentials of all show negative values over most of the pH range and become more negative as the pH increases. This suggests that they are negatively charged in most solutions and the charge density increases with increasing pH. The PDMS treated with PSS exhibits a more negative zeta potential than that treated with UVO and consequently a higher surface charge density. In addition, there is a minor variation (about 3 mV) in the zeta potential of the PSS-treated PDMS before and after UVO treatment, suggesting that the UVO treatment partially damages the PSS modified on the PDMS surface. In future work, we will use low-power plasma treatment to bond PDMS with glass to eliminate interference from the UV/ozone treatment. We perform DC sweep tests on devices fabricated with PSS-treated PDMS using 1 mM KCl solutions of varying pH values. As shown in Fig. 3(d) (inset is the hysteresis area at three pH values), it is observed that an increase in pH value corresponds to a significantly larger hysteresis area during the positive voltage. Since the hysteresis area during the negative voltage is inherently small due to ion depletion, differences between pH values are less noticeable. When using 1 mM KCl solution, the ICR ratio and hysteresis area are smallest at pH 4. This can be attributed to the lowest surface charge density, which weakens the memristive effect and results in an almost linear *I*–*V* curve. At pH 10, the hysteresis area in the negative voltage range is very small, indicating that ion depletion has reached a relative maximum. In contrast, at pH 7, the reverse hysteresis area is larger, suggesting that ion depletion is less pronounced compared to pH 10. These results validate the theoretical analyses of electrokinetic ion transport and underscore the importance of surface charge in the memristive and ICR effects. Significantly, the application of zeta potential measurements can guide the optimization of device performance by predicting ion enrichment and depletion efficiency through the preliminary assessment of surface charge density and its impact on the extent of ion-surface electrostatic interactions.

3.4 The ICR effect

The ICR has been extensively investigated and many factors have been found to influence the ICR behaviors, such as surface charge density, solution concentration and potential scan rate [29–32]. The ICR ratio, defined as the ratio of currents at the same voltage amplitude but opposite polarity, is commonly used to describe the nonlinearity of current–voltage curves or deviations from ohmic conductance. In this study, we use the current value at ±3 V when scanning from +5 to −5 V to derive the ICR ratio. Figures 4(a) and 4(b) show that the ICR ratio decreases at higher scan rates with 1 mM KCl solution, which is qualitatively consistent with previous experimental and computational studies [9, 20]. The ICR at different scan rates in asymmetric charged nanochannels depends on the relatively sluggish ion redistribution, which controls the perm-selective properties of the nanochannel. At low scan rates, most of the current within the nanochannel is carried by cations, demonstrating the perm-selective property (Fig. 4(c)). At high scan rates, the perm-selectivity of the nanochannel is barely established and the nanochannel behaves as an ohmic resistor (Fig. 4(d)). In other words, when a fast voltage sweep is applied, the delayed ion redistribution leads to a decrease in ion enrichment/depletion regions, resulting in a loss of rectification.

Moreover, owing to the direct influence of solution concentration on the thickness of EDL structure, the ICR is strongly dependent on the solution concentration [33]. As shown in Figs. 4(e) and 4(f), the ICR ratio decreases with increasing concentration at a scan rate of 0.07 V/s. At low concentrations, the EDL thickness (λ_1) is large (see detailed analysis in the ESM) and the nanochannel is primarily filled with cations that neutralize the negative surface charge, leading to greater ion enrichment (Fig. 4(g)). In contrast, at high concentrations where the EDL is thin (λ_2), most of the nanochannel volume is filled with bulk solution (Fig. 4(h)). The conductance is governed by the bulk concentration and is not significantly affected by the surface charge density (Table S1 in the ESM) [34]. At this point, the *I*–*V* curve is almost linear and the ICR

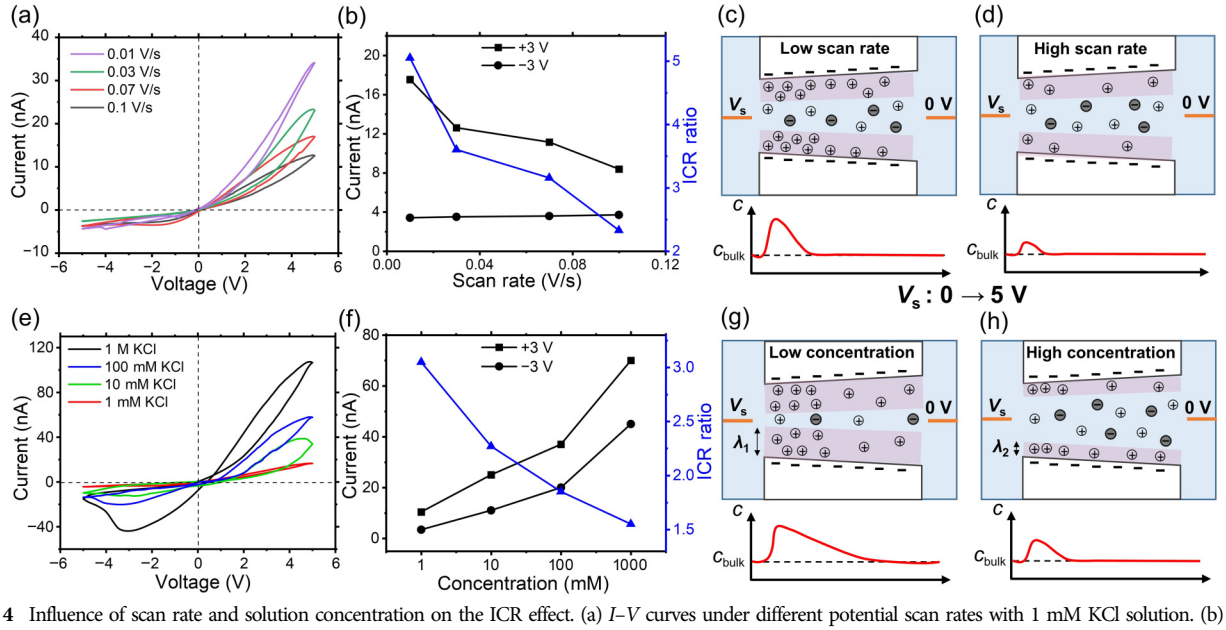

Figure 4 Influence of scan rate and solution concentration on the ICR effect. (a) *I*–*V* curves under different potential scan rates with 1 mM KCl solution. (b) Plot of absolute value of current at ±3 V and ICR ratio versus scan rate. (c) and (d) Schematic of ion redistribution in nanochannels at different scan rates. (e) *I*–*V* curves under different KCl concentrations at a scan rate of 0.07 V/s. (f) Plot of absolute value of current at ±3 V and ICR ratio versus KCl concentration. (g) and (h) Schematic of ion redistribution in nanochannels with different solution concentrations.

ratio is close to one. In addition, by adjusting the ethanol volume during device fabrication, the PDMS nanochannels can be prepared with different widths and channel spacings. The influence of the channel size on the device performance has also been investigated, as shown in Fig. S3 in the ESM. When the average channel width is smaller, such as 150 nm, the curve exhibits the highest degree of nonlinearity and the ICR effect is most pronounced. As the channel width increases, the ICR ratio decreases and the *I*–*V* curve becomes progressively more linear. Simultaneously, the difference in the hysteresis areas between the positive and negative voltage diminishes. When the channel size increases significantly and reaches the micrometer scale, the *I*–*V* curve becomes nearly linear with no self-crossing point, showing only a slight deviation due to water electrolysis, indicating a loss of device functionality. Therefore, it is crucial to control the channel widths within a certain range to realize the memristive effect, with smaller widths generally being more favorable.

3.5 Short-term synaptic plasticity (STP) simulated by PDMS-glass nanofluidic chip

Relying on the basic electrical properties, the PDMS-glass nanofluidic chip exhibits short-term plasticity. As shown in Fig. 5(a), by applying a few continuous triangular-wave pulses (±6 V, 4 ms) to the device, the conductance can be increased and decreased within consecutive pulse signals. This behavior resembles the short-term plasticity of biological neurons, indicating that the device can simulate basic synaptic functions such as paired-pulse facilitation (PPF) and paired-pulse depression (PPD) [35]. As shown in Fig. 5(b) and 5(c), increasing the number of consecutive pulses to 30, the current (conductance) changes rapidly at first and then stabilizes under the last few pulses. With 30 negative pulses, the current change (ΔI) is approximately 9 nA, which is greater than the 5 nA observed with positive pulses. This result suggests that ion depletion under reverse voltage occurs faster and more easily than positive voltage. Consequently, we explore the current changes at different intervals (Δt) between two negative voltage pulses. As shown in Fig. 5(d), shortening the voltage pulse interval (Δt) results in an increased current change (ΔI), whereas a longer voltage pulse interval results in a decreased ΔI. This dynamic decrease mimics the adjustment of synaptic weight in shaping biological short-term plasticity under repeated stimuli of different frequencies [14]. According to the definition of retention in fluidic memristors by Xiong et al. [14], the retention time (t_r) is the pulse interval (Δt) where current change (ΔI) drops to 5% of its maximum ($\Delta I_{\Delta t=t_r} = 5\%\ \Delta I_{\Delta t=0}$). As shown in Fig. 5(d), for a certain voltage pulse stimulation (V = −6 V, the pulse width (t_p) = 4 ms), t_r is calculated to be ~ 5 ms. According to the theory of ion diffusion kinetic, the typical diffusion time scale is roughly L^2/D, where L represents the diffusion distance and D (around 10^{-9} m^2/s) is a typical ionic diffusion coefficient in the channel [16]. As a result, once the voltage pulse is removed, the conductance of our devices reverts to its initial state within milliseconds, hindering the achievement of long-term plasticity. Figure 5(e) illustrates the influence of pulse amplitude on the conductance modulation of the nanofluidic memristor. At smaller amplitudes, such as −2 V, the current at the voltage peak remains almost constant with 30 consecutive negative pulses, indicating that the device conductance remains almost unchanged. However, at larger amplitudes (−4 V and above), the conductance decreases, with larger changes in conductance observed at −6 V. Figure 5(f) shows that as t_p increases, the device conductance increases and with 10 consecutive negative pulses, smaller pulse widths result in greater reductions in device conductance. Here, we estimated the energy consumption per channel using the equation $W = \frac{0.5VIt_p}{N}$, where V = 5 V, $I \approx$ 30 nA and t_p = 4 ms based on the results shown in Figs. 5(b) and 5(c). The number of parallel channels N is 25. Thus, the energy dissipation for a single channel is approximately 12 pJ per spike, which is relatively low for nanofluidic memristors as far as we know (Table S2 in the ESM). These results provide initial evidence that our nanofluidic memristors have promising potential for neuromorphic computing applications.

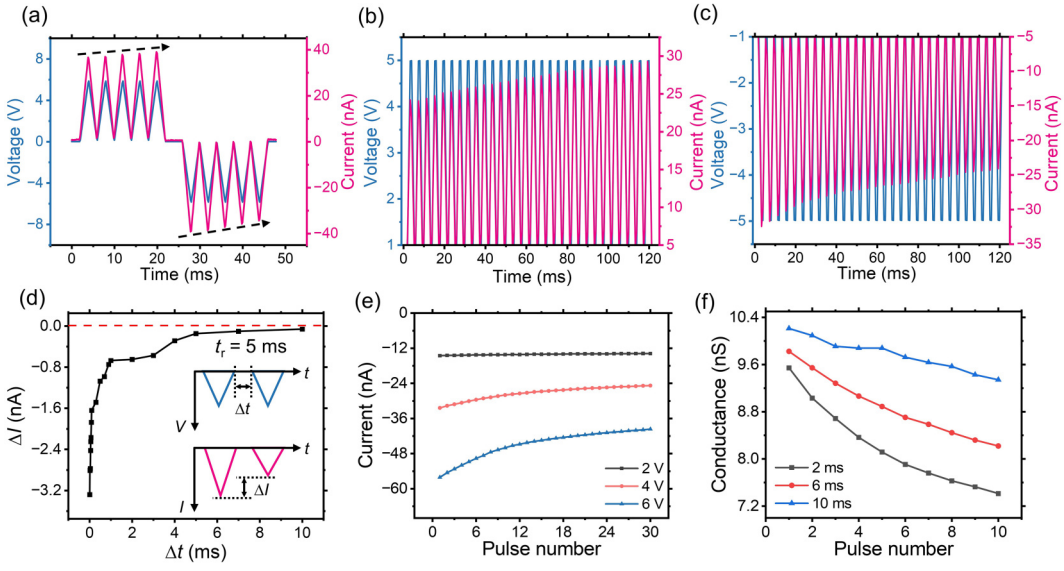

Figure 5 Short-term synaptic plasticity simulated by the nanofluidic memristors. (a) PPF and PPD. Successive positive (negative) pulses (V = ±6 V, t_p = 4 ms, Δt = 0) result in an increase (decrease) in conductance. (b) and (c) Current responses under 30 voltage pulses (V = ±5 V, t_p = 4 ms, Δt = 0). (d) Plot of current changes (ΔI) versus the paired pulse intervals (Δt) under negative voltage pulses (V = −6 V, t_p = 4 ms). (e) Evolution of the current at the voltage peak of the triangular wave under 30 voltage pulses (t_p = 4 ms, Δt = 0) with different pulse amplitudes. (f) Evolution of the conductance under 10 negative pulses (V = −6 V, Δt = 0) with different pulse widths.

4 Conclusions

In this work, we have developed a new nanofluidic memristor, which is a PDMS-glass chip with a pair of Pt electrodes and a nanochannel array for ion enrichment and depletion. The device not only exhibits typical bipolar memristive behavior and ICR but also demonstrates excellent endurance, maintaining stable performance after 100 sweep cycles. We systematically investigate key factors affecting ion transport behavior in this memristive effect, including potential scan rates, solution concentration and surface charge density. The results show that the ICR ratio of the *I*–*V* hysteresis curves decreases with potential scan rate and solution concentration. By introducing zeta potential measurements, we reveal that the PDMS surface becomes more negatively charged in higher pH solutions which can enhance memristive and ICR effects. Furthermore, our memristor has successfully simulated short-term synaptic plasticity, such as PPF and PPD, while achieving a relatively low energy consumption of 12 pJ per spike per channel. In summary, the easily accessible and reliable nanofluidic memristors presented in this study holds promise for accelerating the optimization of device structure and performance, thereby advancing their application in neuromorphic computing.

Electronic Supplementary Material: Supplementary material (theoretical derivation of the ion enrichment/depletion, SEM images of PDMS nanochannels, *I*–*V* curves with 10 mM to 1 M KCl solution and comparisons with other nanofluidic memristors) is available in the online version of this article at https://doi.org/10.26599/NR.2025.94907098.

Data availability

All data needed to support the conclusions in the paper are presented in the manuscript and the Electronic Supplementary Material. Additional data related to this paper may be requested from the corresponding author upon request.

Acknowledgements

This work is supported by the Fundamental Research Funds for the Central Universities (No. 30923010603) and the National Natural Science Foundation of China (No. 62074079).

Declaration of competing interest

All the contributing authors report no conflict of interests in this work.

Author contribution statement

W. L. S.: Experimental design and conduction, data curation, writing manuscript. Y. K. X., P. Y. Y. and F. S.: Data curation, conceptualization. X. Z. and C. X. S.: Validation, supervision. Q. W. and Y. F. Y.: Project administration, funding acquisition, supervision. All the authors have approved the final manuscript.

Use of AI statement

None.

References

[1] Goswami, S.; Pramanick, R.; Patra, A.; Rath, S. P.; Foltin, M.; Ariando, A.; Thompson, D.; Venkatesan, T.; Goswami, S.; Williams, R. S. Decision trees within a molecular memristor. *Nature* **2021**, *597*, 51–56.

[2] Chua, L. Memristor-the missing circuit element. *IEEE Trans. Circuit Theory* **1971**, *18*, 507–519.

[3] Zhu, J. D.; Zhang, T.; Yang, Y. C.; Huang, R. A comprehensive review on emerging artificial neuromorphic devices. *Appl. Phys. Rev.* **2020**, *7*, 011312.

[4] Strukov, D. B.; Snider, G. S.; Stewart, D. R.; Williams, R. S. The missing memristor found. *Nature* **2008**, *453*, 80–83.

[5] Waser, R.; Aono, M. Nanoionics-based resistive switching memories. *Nat. Mater.* **2007**, *6*, 833–840.

[6] Lanza, M.; Sebastian, A.; Lu, W. D.; Gallo, M. L.; Chang, M. F.; Akinwande, D.; Puglisi, F. M.; Alshareef, H. N.; Liu, M.; Roldan, J. B. Memristive technologies for data storage, computation, encryption, and radio-frequency communication. *Science* **2022**, *376*, eabj9979.

[7] Wang, Z. R.; Wu, H. Q.; Burr, G. W.; Hwang, C. S.; Wang, K. L.; Xia, Q. F.; Yang, J. J. Resistive switching materials for information processing. *Nat. Rev. Mater.* **2020**, *5*, 173–195.

[8] Zhang, J. R.; Liu, W. C.; Dai, J. Q.; Xiao, K. Nanoionics from biological to artificial systems: An alternative beyond nanoelectronics. *Adv. Sci.* **2022**, *9*, 2200534.

[9] Guerrette, J. P.; Zhang, B. Scan-rate-dependent current rectification of cone-shaped silica nanopores in quartz nanopipettes. *J. Am. Chem. Soc.* **2010**, *132*, 17088–17091.

[10] Wang, D. C.; Kvetny, M.; Liu, J.; Brown, W.; Li, Y.; Wang, G. L. Transmembrane potential across single conical nanopores and resulting memristive and memcapacitive ion transport. *J. Am. Chem. Soc.* **2012**, *134*, 3651–3654.

[11] Zhang, P.; Xia, M.; Zhuge, F. W.; Zhou, Y.; Wang, Z. Y.; Dong, B. Y.; Fu, Y. Y.; Yang, K. C.; Li, Y.; He, Y. H. et al. Nanochannel-based transport in an interfacial memristor can emulate the analog weight modulation of synapses. *Nano Lett.* **2019**, *19*, 4279–4286.

[12] Najem, J. S.; Taylor, G. J.; Weiss, R. J.; Hasan, M. S.; Rose, G.; Schuman, C. D.; Belianinov, A.; Collier, C. P.; Sarles, S. A. Memristive ion channel-doped biomembranes as synaptic mimics. *ACS Nano* **2018**, *12*, 4702–4711.

[13] Bu, Y.; Ahmed, Z.; Yobas, L. A nanofluidic memristor based on ion concentration polarization. *Analyst* **2019**, *144*, 7168–7172.

[14] Xiong, T. Y.; Li, C. W.; He, X. L.; Xie, B. Y.; Zong, J. W.; Jiang, Y. N.; Ma, W. J.; Wu, F.; Fei, J. J.; Yu, P. et al. Neuromorphic functions with a polyelectrolyte-confined fluidic memristor. *Science* **2023**, *379*, 156–161.

[15] Robin, P.; Kavokine, N.; Bocquet, L. Modeling of emergent memory and voltage spiking in ionic transport through angstrom-scale slits. *Science* **2021**, *373*, 687–691.

[16] Robin, P.; Emmerich, T.; Ismail, A.; Niguès, A.; You, Y.; Nam, G. H.; Keerthi, A.; Siria, A.; Geim, A. K.; Radha, B. et al. Long-term memory and synapse-like dynamics in two-dimensional nanofluidic channels. *Science* **2023**, *379*, 161–167.

[17] Xu, B. Y.; Xu, J. J.; Xia, X. H.; Chen, H. Y. Large scale lithography-free nano channel array on polystyrene. *Lab Chip* **2010**, *10*, 2894–2901.

[18] Peng, R.; Li, D. Q. Fabrication of polydimethylsiloxane (PDMS) nanofluidic chips with controllable channel size and spacing. *Lab Chip* **2016**, *16*, 3767–3776.

[19] Cheng, L. J.; Guo, L. J. Ionic current rectification, breakdown, and switching in heterogeneous oxide nanofluidic devices. *ACS Nano* **2009**, *3*, 575–584.

[20] Momotenko, D.; Girault, H. H. Scan-rate-dependent ion current rectification and rectification inversion in charged conical nanopores. *J. Am. Chem. Soc.* **2011**, *133*, 14496–14499.

[21] Adhikari, S. P.; Sah, M. P.; Kim, H.; Chua, L. O. Three fingerprints of

memristor. In *Handbook of Memristor Networks*. Chua, L.; Sirakoulis, G. C.; Adamatzky, A., Eds.; Springer: Cham, 2019; pp 165–196.
[22] Lim, A. E.; Lim, C. Y.; Lam, Y. C. Electroosmotic flow hysteresis for dissimilar ionic solutions. *Biomicrofluidics* **2015**, *9*, 024113.
[23] Zhao, C. L.; Yang, C. Advances in electrokinetics and their applications in micro/nano fluidics. *Microfluid. Nanofluid.* **2012**, *13*, 179–203.
[24] Wang, D. C.; Brown, W.; Li, Y.; Kvetny, M.; Liu, J.; Wang, G. L. Correlation of ion transport hysteresis with the nanogeometry and surface factors in single conical nanopores. *Anal. Chem.* **2017**, *89*, 11811–11817.
[25] Wang, D. C.; Liu, J.; Kvetny, M.; Li, Y.; Brown, W.; Wang, G. L. Physical origin of dynamic ion transport features through single conical nanopores at different bias frequencies. *Chem. Sci.* **2014**, *5*, 1827–1832.
[26] Wang, D. C.; Brown, W.; Li, Y.; Kvetny, M.; Liu, J.; Wang, G. L. Hysteresis charges in the dynamic enrichment and depletion of ions in single conical nanopores. *ChemElectroChem* **2018**, *5*, 3089–3095.
[27] Liu, Z.; Liu, X. Y.; Wang, Y. F.; Yang, D. F.; Li, C. Z. Ion current rectification in asymmetric charged bilayer nanochannels. *Electrochim. Acta* **2022**, *403*, 139706.
[28] Liu, Z. L.; Hedayati, P.; Sudhölter, E. J. R.; Haaring, R.; Shaik, A. R.; Kumar, N. Adsorption behavior of anionic surfactants to silica surfaces in the presence of calcium ion and polystyrene sulfonate. *Colloids Surf. A: Physicochem. Eng. Asp.* **2020**, *602*, 125074.
[29] Tseng, S.; Lin, S. C.; Lin, C. Y.; Hsu, J. P. Influences of cone angle and surface charge density on the ion current rectification behavior of a conical nanopore. *J. Phys. Chem. C* **2016**, *120*, 25620–25627.
[30] Yusko, E. C.; An, R.; Mayer, M. Electroosmotic flow can generate ion current rectification in nano- and micropores. *ACS Nano* **2010**, *4*, 477–487.
[31] Lan, W. J.; Holden, D. A.; White, H. S. Pressure-dependent ion current rectification in conical-shaped glass nanopores. *J. Am. Chem. Soc.* **2011**, *133*, 13300–13303.
[32] Siwy, Z. S. Ion-current rectification in nanopores and nanotubes with broken symmetry. *Adv. Funct. Mater.* **2006**, *16*, 735–746.
[33] Xiong, T. Y.; Zhang, K. L.; Jiang, Y. N.; Yu, P.; Mao, L. Q. Ion current rectification: From nanoscale to microscale. *Sci. China Chem.* **2019**, *62*, 1346–1359.
[34] Schoch, R. B.; van Lintel, H.; Renaud, P. Effect of the surface charge on ion transport through nanoslits. *Phys. Fluids* **2005**, *17*, 100604.
[35] Yang, R.; Huang, H. M.; Guo, X. Memristive synapses and neurons for bioinspired computing. *Adv. Electron. Mater.* **2019**, *5*, 1900287.